Predicting kinetics of polymorphic transformations from structure mapping and coordination analysis

Vladan Stevanović, Ryan Trottier, Charles Musgrave, Félix Therrien, Aaron Holder, and Peter Graf

Phys. Rev. Materials **2**, 033802 — Published 26 March 2018

DOI: 10.1103/PhysRevMaterials.2.033802

Predicting kinetics of polymorphic transformations from structure mapping and coordination analysis

Vladan Stevanović*
Colorado School of Mines, Golden, Colorado 80401, USA and
National Renewable Energy Laboratory, Golden, Colorado 80401, USA

Ryan Trottier and Charles Musgrave
University of Colorado Boulder, Colorado 80309, USA

Félix Therrien
Colorado School of Mines, Golden, Colorado 80401, USA

Aaron Holder
National Renewable Energy Laboratory, Golden, Colorado 80401, USA and
University of Colorado Boulder, Colorado 80309, USA

Peter Graf
National Renewable Energy Laboratory, Golden, Colorado 80401, USA
(Dated: February 27, 2018)

To extend materials design and discovery into the space of metastable polymorphs, rapid and reliable assessment of transformation kinetics to lower energy structures is essential. Herein we focus on diffusionless polymorphic transformations and investigate routes to assess their kinetics using solely crystallographic arguments. As part of this investigation we developed a general algorithm to map crystal structures onto each other, and ascertain the low-energy (fast-kinetics) transformation pathways between them. Pathways with minimal dissociation of chemical bonds, along which the number of bonds (in ionic systems the first-shell coordination) does not decrease below that in the end structures, are shown to always be the fast-kinetics pathways. These findings enable the rapid assessment of the kinetics of polymorphic transformation and the identification of long-lived metastable structures. The utility is demonstrated on a number of transformations including those between high-pressure SnO_2 phases, which lack a detailed atomic-level understanding.

Keywords: polymorphism, metastability, phase transformations, structure prediction

I. INTRODUCTION

The strong dependence of physical properties on crystal structure offers compelling opportunities for discovering new functional materials among metastable polymorphs. The search for new and useful metastable structures however, critically requires: (*i*) accurate and efficient structure and property prediction algorithms to screen the potential energy surface (PES) for polymorphs with desirable properties, and (*ii*) rapid and reliable assessment of the kinetics of transformations to lower energy states to identify long-lived polymorphs among the multitude of possible low-energy structures. With the advent of total energy methods considerable efforts have been devoted to the former problem. As a result, a range of structure prediction methods were developed[1–3] and successfully combined with property predictions[4–11].

In the context of metastability and polymorphism, identification of bonafide metastable structures among tens if not hundreds of low-energy structures that typically result from structure predictions[12,13] remains a significant challenge[14]. Recently discovered correlation between volumes of configuration space occupied by different PES local minima (their basins of attraction) and experimentally realized metastable structures[15–17] offers guidance in narrowing down the list of candidate metastable structures. However, when targeting metastable forms of matter, knowledge of the kinetics of transformations to lower energy states is invaluable.

Kinetics of polymorphic transformations is often described in terms of the minimum energy transformation pathways and associated activation energies, that is, energies of the saddle points (transition states) along the pathway. Efforts in developing computational approaches to predict minimum energy pathways between *periodic* structures, find saddle points and their energy have also been (and still are) under development. The generalized solid-state nudged elastic band (ssNEB) formalism[18–20] enables a unified description of the atomic and structural degrees of freedom along a polymorphic transformation pathway. While the ssNEB algorithm itself can be efficient, the computational cost of the underlying electronic structure calculations and complexities in choosing the best initial pathway limit its use for rapid identification of long-lived, metastable polymorphs.

A method that could examine large sets of polymorphs, even if offering only a semi-quantitative assessment, would greatly benefit metastable polymorph discovery. One such attempt can be found in the work of

Buerger[21], who classified polymorphic transformations as *slow* or *rapid* using mainly crystallographic arguments. In short, the existence of a diffusionless (displacive or dilatational) transformation between two structures is, according to Buerger, a signature of fast kinetics. One transformation that disobeys this classification is diamond to graphite for which Buerger devised an additional class of transformations of the bond type, covalent to metallic in this case, which he argued should be slow irrespective of geometry. The main limitation of the Buerger's classification scheme is that it can only be applied to transformations for which the mechanism is already known.

Motivated by the Buerger's work, we investigate in this paper routes to assess kinetics of polymorphic transformations using solely crystallographic arguments. The key component of our work is an algorithm to map crystal structures onto each other, and find diffusionless transformations between them (see Fig. 1). The algorithm relies on two basic principles: (a) minimization of the total Euclidian distance atoms need to travel between the end structures, and (b) minimization of the change in coordination of atoms in the first coordination shell (number of atoms in the first shell) along the map. In other words, the goal is to find an optimal mapping that is diffusionless in nature and which minimizes dissociation of chemical bonds. The developed algorithm successfully reproduces known transformation pathways including $fcc \rightarrow bcc$, diamond $\rightarrow$ graphite, CsCl-type $\rightarrow$ rocksalt, etc. Beyond simple and well studied transformations, we applied our mapping algorithm to study polymorphic transformations between various SnO_2 high-pressure phases for which a detailed atomistic picture is presently elusive.

We will show that if only a qualitative classification into *slow* or *rapid* (à la Buerger) is sufficient, the condition of minimal dissociation of chemical bonds along the pathway can be used as a signature of fast kinetics. More precisely, if a diffusionless pathway can be found along which the number of chemical bonds never decreases below the number of bonds in the end structures, the kinetics of the transformation between the corresponding polymorphs can reliably be classified as *rapid*. Lastly, if a more accurate assessment is necessary, our mapping algorithm is demonstrated to provide a good starting point for subsequent solid-state nudged elastic band (ssNEB) calculations.

Similarly to other methods[18–20,22], in our work we draw conclusions about the kinetics of polymorphic transformations from the assumed collective (concerted) motion of atoms. While phase transitions in solids occur mainly via nucleation and growth, we adopt the view that the features of collective transformations can provide useful insights into the overall kinetics and can serve as the starting point for more realistic modeling of nucleation processes.

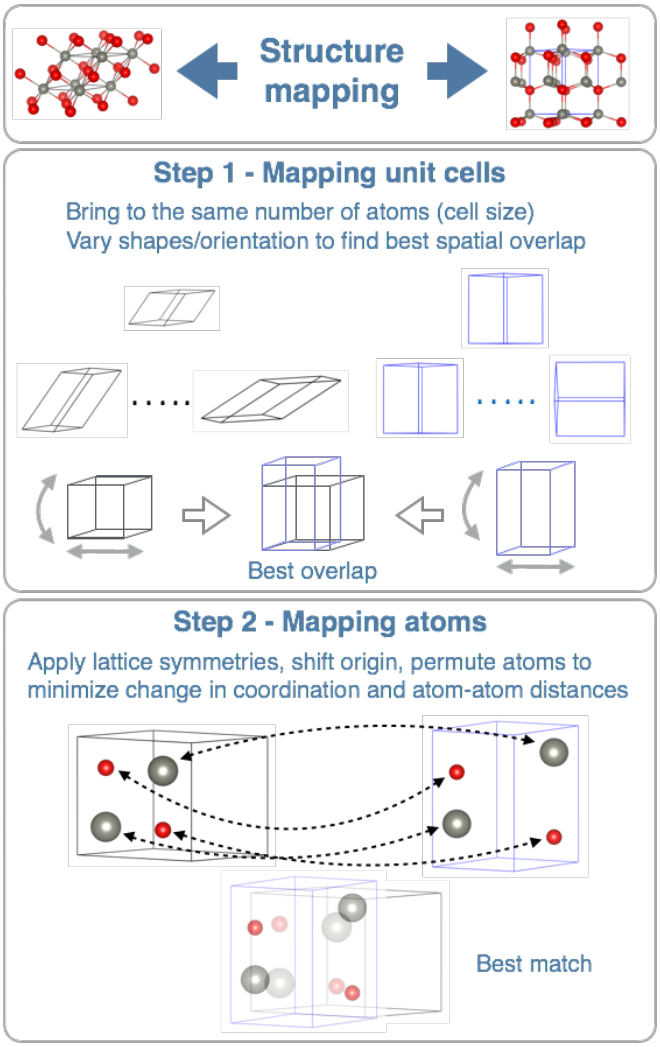

FIG. 1. Schematics of the two step, structure mapping algorithm developed in this work (see text for details).

II. METHODS

A. Structure mapping algorithm

The developed structure mapping algorithm consists of two steps as illustrated in Fig. 1. In the first step the algorithm searches for the most compatible representations of the two structures, that is the optimal mapping of their unit cells. This is done in the following way. The two primitive unit cells are brought to the same – least common multiple – number of atoms by constructing all symmetry inequivalent supercells. The enumeration of the symmetry inequivalent supercells given the number of atoms is done using Hart-Forcade theory[23]. The most compatible representations are then defined by the pair of supercells that minimizes the strain between them, or, in other words, the two supercells with the largest spatial (volumetric) overlap. This condition can be formulated as searching for the pair of unit cells that minimizes the

metric defined as the weighted sum of the absolute differences in unit cell parameters $(a, b, c, \alpha, \beta, \gamma)$ and the total surface areas (S) of the two cells:

$$d(cell_1, cell_2) = \sum_{\substack{q=a,b,c,\\ \alpha,\beta,\gamma,S}} C_q \, |q_1 - q_2|, \qquad (1)$$

where C_q represent positive weights of quantities q that are introduced solely to make the numerical values the same order of magnitude. The search is accomplished by transforming the cells to the corresponding (unique) reduced cell according to the formulation of Niggli-Santoro-Gruber[24–26], which allows implicitly exploring all permutations of the unit cell vectors and all isometric transformations of the two cells (rigid rotations and reflections) to bring them to the positions of largest spatial overlap, as shown in Fig. 1.

In the second step, the atoms are placed back inside the two cells. The optimal atom-to-atom mapping is then searched for by performing the following operations on the two sets of atomic positions: (*i*) all symmetry operations of the parent Bravais lattices, (*ii*) translations of the origin of coordinate frame to each atom site, and (*iii*) permutations of indices of chemically identical atoms. Every choice of symmetry operation, position of the origin, and the permutation of atom indices defines a single mapping between the two end structures and a pathway in configuration space that connects the atoms with same indices and continuously deforms the unit cell.

Out of many possible atom-to-atom mappings our algorithm selects as the optimal mapping the solution that yields minimal dissociation of chemical bonds, i.e., the coordination of atoms along the pathway does not decrease below the coordinations in the end structures. If such a mapping cannot be found, then the one that minimizes the sum of Euclidian distances between the corresponding atoms in the two structures is chosen. Finally, if more than one solution is found with the appropriate change in coordination then the sum of distances between the atoms is used to rank them and narrow down the choice. To achieve this, the described operations are performed using Hart-Forcade theory[23] that allows enumeration of the symmetry inequivalent atom sites. The Hungarian Algorithm of Kuhn and Munkres[27] is used to find the optimal permutation of atom indices (job scheduling problem) in polynomial time.

Ideally, the globally best atom-to-atom mapping would always be found in the unit cell pairing with highest overlap, but this is not the case in general. Therefore, in the first step, we form a list of the top N unit cell pairing (e.g. N=10) and perform the second step on all of them. In practice this has been found to yield the desired globally optimal atom-to-atom mapping.

A similar approach was developed previously by Sadeghi and Goedecker[28] for the purpose of measuring configuration space distances between non-periodic systems. Also, Lonie and Zurek[29] developed a search algorithm designed to identify identical (duplicate) periodic structures which involves mapping of the unit cells. Another class of recently developed approaches utilize the descriptor/feature based fingerprinting to quantify similarity of different periodic structures by comparing selected set of features (not atom-by-atom). These include the work of Yang et al.[30] and Zhu et al.[31]. Our mapping of the unit cells can be viewed as a generalization of the ideas of Lonie and Zurek[29] to the case where input structures are presumed to be different and where the goal is to discover the optimal alignment of the two structures. Concerning the atom-to-atom mapping, we extended the algorithm of Sadeghi and Goedecker[28] to periodic systems. Another important distinguishing feature of our approach is the new objective function, which includes the physical principle of the minimal dissociation of chemical bonds.

Our structure mapping algorithm is available via github as part of the pylada software package[32].

B. Coordination analysis

Along the transformation pathways the symmetry of the end structures is broken, and the distances between the atoms and their first neighbors are not all the same. This poses problems when determining first shell coordination of atoms for intermediate structures. The calculated number of neighbors will in general depend on the cutoff radii and/or tolerances imposed on the distances. In this work we focus on binary ionic systems for which we define the first coordination shell as consisting of the atoms of the type other than the central atom that are all separated from the central atom within a certain tolerance. In other words, the tolerance factor represents the thickness of a spherical shell around the central atom. The first shell is then defined as the number of atoms of the other type that are found inside this shell. The counting starts from the closest atom and stops if either the tolerance or the atom of the same type as the central one is reached, whichever comes first. We check the stability of all our results by varying the tolerance between 0.1 and 0.5 Å.

C. Total energy and ssNEB calculations

All calculations were performed by employing relatively standard DFT computations explained in details elsewhere[33]. In short, the PBE form of the exchange-correlation functional[34] was used within the projector augmented wave (PAW) method[35] as implemented in the VASP code[36]. In case of elemental carbon, the VASP code implementation of the optB86 exchange-correlation functional[37], which includes contributions arising from van der Waalls interactions, was employed. To generate energy profiles along the mapping (pathway) all initial and final structures were fully relaxed (volume, cell shape and atomic coordinates), whereas only the static calcu-

lations were performed for the intermediate structures along the pathway.

The solid state nudged elastic band (ssNEB) calculations were performed using the implementation in the Transition State Tools for VASP (VTST) code developed by the Henkelman group at UT Austin.[19] Each ssNEB calculation was initialized with an approximately 20 image band determined by taking an interpolation of the entire desired polymorphic transformation generated by the mapping algorithm discussed in this paper. The initial pathway is relaxed until the forces on all images were less than 0.01 eV/Å. If any intermediates appeared along the ssNEB, these were relaxed using a standard geometry relaxation, and the ssNEB path was split, taking the intermediate as a new end point for one ssNEB, and a starting point for another. This was done so that each ssNEB calculation would only have a single local maximum. Images were either added or removed from the chain so that each intermediate ssNEB had 10-12 images. Once the NEB images were relaxed, the climbing image NEB method was used to better identify the true saddle point.[38]

III. RESULTS AND DISCUSSION

We tested our structure mapping algorithm on a number of well-studied polymorphic transformations in elemental and simple binary systems, some of which are listed in Table I. The space groups of the lowest symmetry structures that occur along the pathway are also shown. The transformation pathways from Table I reproduce well the maximal symmetry transition paths for the reconstructive phase transitions derived by Capillas et al.[22]. Further, our algorithm often finds the pathway that preserves the largest common subgroup of the two structures. This is a consequence of the supercell sizes chosen to accommodate the least common multiple number of atoms. If this condition is relaxed and larger supercells with compatible numbers of atoms are considered, our algorithm would also find lower symmetry pathways, some of which have been discussed previously for the transformations from Table I. The details of the transformations from Table I are provided in the supplementary materials.

A. Ionic systems: Change in the coordination of atoms and its relevance to the magnitude of kinetic barriers

Another important finding that emerged during the development of our algorithm is that the two conditions, minimal distance between the corresponding atoms in the two structures and minimal change in coordination, do not always coincide. The test cases from Table I revealed the critical significance of the change in coordination. For example, minimizing the distance alone does not necessarily result in the best pathway in the case of *bcc* to *hcp* transformation as there are multiple possible mappings with nearly degenerate distance values, but different coordination of atoms along the pathway. The transformations between the ground state and high temperature tin-sulfide polymorphs, Pnma and Cmcm, also exhibit similar features (see supplementary materials). The condition itself has been referred to previously in case-by-case studies (e.g. Refs.[39,40]) and has a relatively simple physical interpretation. It reflects the requirement of minimizing the number of broken bonds in going from one end structure to the other, which is expected to be correlated with the magnitude of the kinetic barriers.

TABLE I. List of studied polymorphic transformations in elemental and simple binary systems. Space groups of the initial and final structures are given together with lowest symmetry intermediate structures.

FCC ($Fm\bar{3}m$)	→	I4/mmm	→	BCC ($Im\bar{3}m$)
BCC ($Im\bar{3}m$)	→	Cmcm	→	HCP ($P6_3/mmc$)
diamond ($Fd\bar{3}m$)	→	C2/m	→	graphite ($P6_3/mmc$)
CsCl-type ($Pm\bar{3}m$)	→	$R\bar{3}m$	→	rocksalt ($Fm\bar{3}m$)
rocksalt ($Fm\bar{3}m$)	→	$Cmc2_1$	→	wurtzite ($P6_3mc$)
zincblende ($F\bar{4}3m$)	→	Imm2	→	rocksalt ($Fm\bar{3}m$)

We illustrate the correlation between the change in the first shell coordination and the potential energy profile by analyzing the rocksalt ($Fm\bar{3}m$) → wurtzite ($P6_3mc$) transformation in binary ionic systems GaN, ZnO, MgO, and CdO. In the upper part of Fig. 2 five snapshots along the pathway are shown viewed from the wurtzite *c*-axis. In the middle part, potential energy profiles along the pathway are shown. They are calculated using density functional theory (DFT). The energy axis is relative to each ground state structure, wurtzite for GaN and ZnO and rocksalt for MgO and CdO. For every chemical composition the end structures are fully relaxed (volume, cell shape and atomic positions), while the total energies of the snapshots along the pathway are computed without any relaxations. For each system the pathways are discretized into 100 equally spaced successive snapshots shown in Fig. 2. We employ a relatively standard DFT-GGA numerical setup described in Section II C.

As evident from Fig. 2 for all four systems calculated energy profiles exhibit relatively small barriers for transformation from the higher energy into the corresponding ground state state structure, which corresponds well to the known, fast kinetics of this transformation[41,42]. The highest energy points along the pathways are all below 100 meV/atom, which is usually considered low activation energy[43]. Because the calculated energy profiles can be thought of as providing the upper bounds for the true activation energies, this result shows that irrespective of the chemistry, this particular transformation is associated with relatively low energy barriers. In addition, the change in coordination of the atoms from the

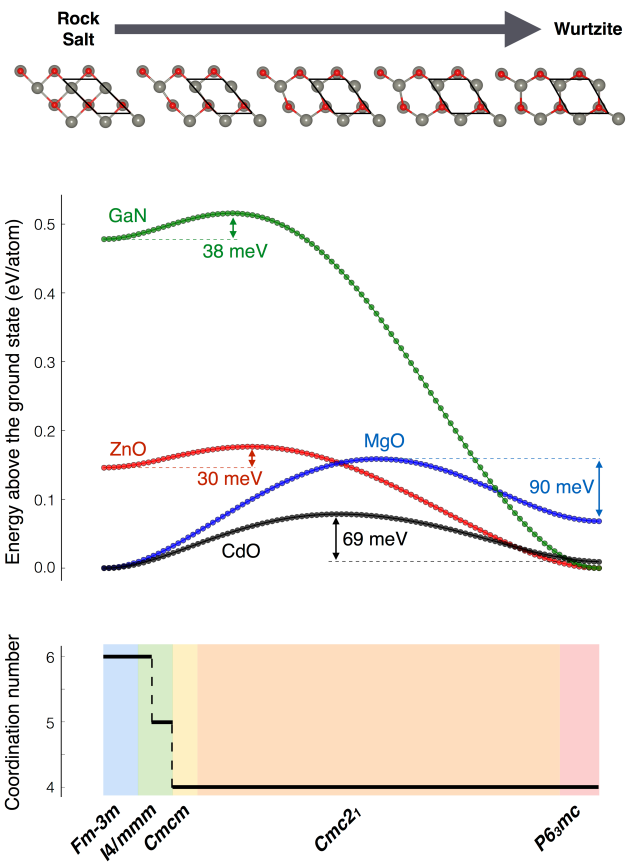

FIG. 2. Five snapshots along the rocksalt ($Fm\bar{3}m$) → wurtzite ($P6_3mc$) transformation are shown (upper) together with the energy profiles (middle) and the change in coordination along the pathway (lower). The invisible x-axis represents normalized reaction coordinate.

6-fold coordinated rocksalt phase to 4-fold coordinated is evidently monotonic, i.e. only the absolutely necessary number of bonds dissociate along the pathway, which is consistent with the above discussion. Similar results are obtained for other transformations from Table I including: BCC → HCP in metallic titanium for which we find a nearly barrierless energy profile in line with previous findings[43]; CsCl-type → rocksalt in CsCl, with the monotonic change in coordinations and the upper bound for the activation energy of 13 meV/atom. Moreover, for the zincblende → rocksalt transformation in SiC our algorithm confirms previously discussed energetic preference of the orthorhombic (Imm2) pathway relative to the R3m mechanism because of the monotonic change in the coordination of atoms from four to six[39,40]. The calculated energy profiles peak at 112 and 250 meV/atom for the pathways passing through the Imm2 and R3m, respectively, in agreement with previous studies.

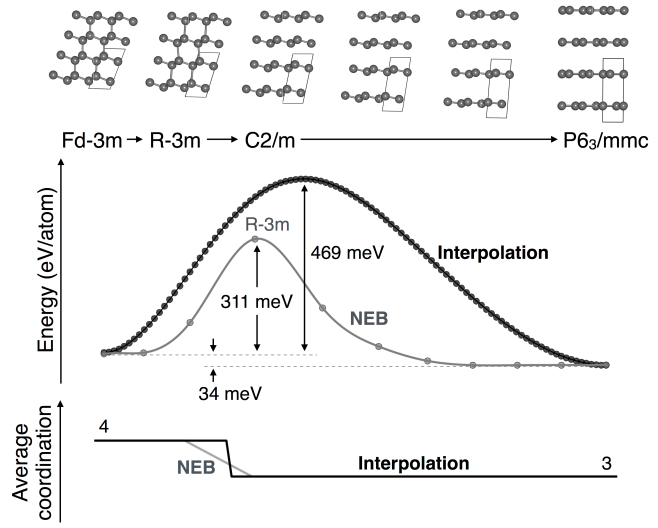

FIG. 3. Snapshots along the diamond to graphite transformation are shown together with the space group symmetry, calculated energy profiles and the evolution of the coordination number. Two energy profiles calculated using the discretized pathway produced by our algorithm (black) and the ssNEB result (grey) are shown as well as the corresponding coordination numbers colored in the same way.

B. Covalent systems: Diamond → Graphite transformation

Our results also confirm the exception to the rule, the cubic diamond → hexagonal graphite transformation for which our algorithm finds the same transformation pathway as the one discussed in Refs.[44,45] that is accompanied by a monotonic change in coordination of atoms (see Fig. 3) and yet, the maximal energy point along the pathway is ∼ 470 meV/atom above the diamond structure. Similar to other systems studied herein, the calculations were performed by discretizing the pathway constructed by our algorithm (interpolation). Fig. 3 also illustrates the energy profile in grey, which resulted from the ssNEB calculation that used our mapping algorithm pathway as the initial pathway. As expected, the calculated ssNEB energy barrier is lower, but the qualitative picture does not change. The transformation is slow despite the monotonic change in coordination reproduced by both sets of calculations.

So, why is elemental carbon different? As correctly observed by Buerger, the diamond to graphite transformation requires a change in chemical bonding. In the diamond structure the four carbon sp^3 hybrid atomic orbitals form four strong σ bonds per carbon atom. These are replaced in the graphite structure by three sp^2 hybrids, which form three σ bonds per carbon, and a p_z orbital, which forms one weaker, resonating π bond per carbon. Relatively weak Van der Waals interactions between the layers further stabilize the graphite structure. If one counts the number of chemical bonds per atom

rather than the geometric coordination, then both diamond and graphite have four bonds per carbon atom and the transformation from diamond to graphite would imply dissociation and formation of one bond per C. Consistent with the previous discussion, the intermediate decrease in the number of chemical bonds to three from four in the end structures would lead to a high barrier.

In ionic systems on the other hand, significant contribution to the energy differences between different atomic configurations comes form purely electrostatic interactions[46,47]. Hence, the increase in energy along the pathway is influenced by the changes in the charge distribution and to a lesser extent is due to vanishing overlaps of atomic overlaps. The evidence of the remaining charge transfer along the pathways are the non-vanishing bandgaps for all ionic systems studied here. Therefore, the argument here is that the geometric coordination of atoms along the pathway is more appropriate when trying to understand the kinetics of polymorphic transformations in ionic systems, while in covalent systems it needs to be replaced by a chemical bonding analysis. In both cases however, the condition of minimal dissociation of chemical bonds serves as a signature of rapid transformations.

C. SnO_2 polymorphs

To further validate the previous discussion we extend our study to SnO_2, a partially ionic system for which a number of polymorphs have been realized under pressure. With increasing pressure the structures appear in the following sequence: $P4_2/mnm \rightarrow Pnnm \rightarrow Pbcn \rightarrow Pa3 \rightarrow Pbca \rightarrow Fm\bar{3}m$[48,49]. Upon releasing the pressure, however, all phases either relax back to the ground state rutile ($P4_2/mnm$) structure following the same sequence or to a phase mixture between rutile and the Pbcn structure (α-PbO_2 structure type)[49,50]. So, the only phase that survives at ambient conditions is $P4_2/mnm$, occasionally in combination with small amounts of Pbcn. A previous study[16] has shown that these two SnO_2 structures, $P4_2/mnm$ and Pbcn, have the "largest" local minima, that is, they occupy larger regions of configuration space than any other. Here, we extend this result by investigating transition pathways between different SnO_2 polymorphs.

In Fig. 4, a chart illustrating the crystal structures of all six SnO_2 polymorphs is shown with thick arrows connecting structures for which our structure mapping and coordination analysis suggest fast polymorphic transformations. The arrows point in the direction of lowering total energy. Interestingly, the highest pressure $Fm\bar{3}m$ phase is connected to all other phases by a fast polymorphic transformation. The DFT calculated energy profiles all exhibit energy barriers lower than 30 meV/atom[51]. Hence, upon releasing the pressure the $Fm\bar{3}m$ structure can, depending on the actual barriers and other factors such as how fast the pressure is released or defects in the material, transform relatively quickly to

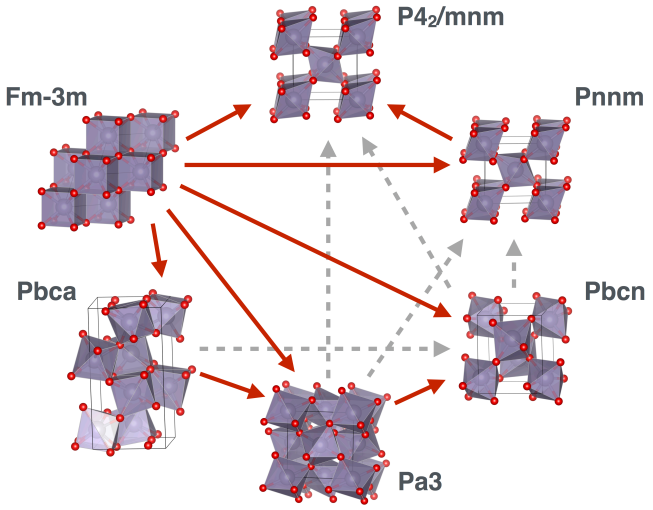

FIG. 4. Map of six SnO_2 polymorphs. Thick arrows indicate *fast* polymorphic transformations as predicted by our structure mapping and coordination analysis. Arrows go in the direction of lowering energy. Dashed arrows indicate transformations for which the change in coordination depends strongly on the distance cutoff used (see text). The missing arrows correspond to transformations predicted to be *slow*.

any of the other SnO_2 polymorph structures upon releasing pressure. This semi-quantitative assessment is consistent with the observations from the high-pressure experiments.[49,50]

We also find another classe of transformations between the SnO_2 polymorphs, those marked in Fig. 4 by dashed arrows. For these transformations our classification based on the coordination analysis is very sensitive on the tolerance used in evaluating the coordination of atoms (see Section II B). The dashed arrows in Fig. 4 represent the transformation pathways that would either be classified as slow for the smallest tolerance factor (0.1 Å) and would change to fast upon increasing the tolerance, or for which the results would be ambiguous, *i.e.,* the trends in the coordination of different types of atoms would be different (opposite). The former physically means that along the pathway some chemical bonds are strained more than others, but the atoms remain relatively close to each other. The latter means that the atoms of the same type as the central atom approached closer to the central atom and intermixed with its first coordination shell and in that way decreased the evaluated coordination number. Based on the subsequent ssNEB calculations we argue that it is more appropriate to classify these types of transformations as likely rapid for the following reason. Namely, our procedure is based solely on geometry and does not allow atoms to relax to more stable configurations as, for example, the ssNEB method would. Therefore, because of the energy minimization with respect to atomic positions within the ssNEB the atoms will have the opportunity to re-bond during the atomic relaxations, which would then lower the barrier

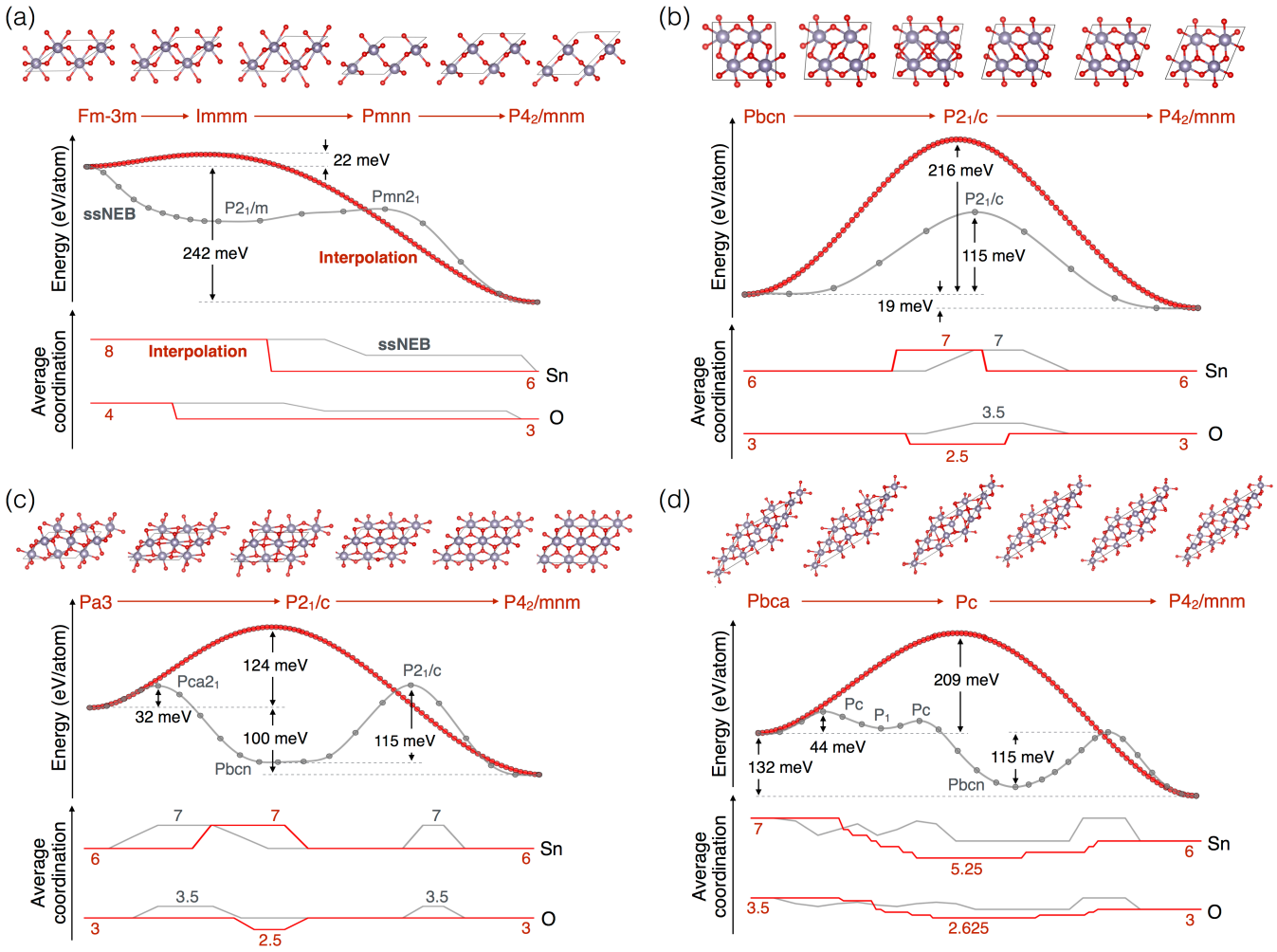

FIG. 5. Calculated energy profiles are shown (in red) for the four selected polymorphic transformations from Fig. 4 together with the space group symmetry, five crystal structure snapshots along the pathway and the average coordination of Sn and O. The corresponding ssNEB results are shown in grey. The x-axis represents the normalized reaction coordinate.

and imply fast transformation based on the coordination analysis. Based on this discussion, all dashed-line transformations from Fig. 4 should be classified as rapid.

Finally, the coordination analysis along the Pbca → $P4_2/mnm$ and Pbca → Pnnm pathways clearly shows the dissociation of chemical bonds and consequently, we do not connect these structures with arrows. Unlike those marked by the dashed arrows, the change in coordination along Pbca → $P4_2/mnm$ and Pbca → Pnnm does not depend on the details of how is the first shell coordination of atoms evaluated.

To better illustrate previous discussion we show in Fig. 5 calculated energy profiles and the average coordination of atoms along the pathways together with the ssNEB results for a selected set of transformations from Fig. 4. We consider $Fm\bar{3}m$ → $P4_2/mnm$ (thick arrow), Pbcn → $P4_2/mnm$ (dashed arrow), Pa3 → $P4_2/mnm$ (dashed arrow), and Pbca → $P4_2/mnm$ (no arrow). The first transformation, which would be classified as fast according to our coordination analysis, clearly indicates the existence of a low energy barrier. The highest energy point along the pathway is only 22 meV/atom above the high-pressure $Fm\bar{3}m$ phase. The transformation is nearly barrierless in the ssNEB showing a very similar change in the coordination of atoms. The second and third transformations that are denoted by dashed arrows in Fig. 4 both fall in the category of undetermined based on the initial coordination analysis. Namely, the coordination numbers for Sn and O follow opposite trends. While the coordination of Sn grows along the pathway from six to seven the average number of first shell Sn atoms surrounding oxygen drops from 3 to 2.5. The reason for this is already mentioned intermixing of O atoms within the first shell of other O atoms, which decreases their first shell coordination number (as defined here) and increases Sn coordination numbers. Minimization of energy within the ssNEB formalism would allow for some rearrangements of atoms and lowering of the energy barriers

along these pathways. Indeed, the energy barriers calculated from the direct interpolation along our pathways are about 216 and 124 meV/atom for Pbcn → $P4_2/mnm$ and Pa3 → $P4_2/mnm$, respectively. The subsequent ssNEB calculations lower the energy barriers in both cases, but while for the Pbcn → $P4_2/mnm$ the symmetry of the initial pathway remains the same with the final barrier of 115 meV/atom, the ssNEB result for the Pa3 → $P4_2/mnm$ relaxes from the initial pathway to the one that has the Pbcn structure as the intermediate. The ssNEB energy barrier for the Pa3 → Pbcn transition is 32 meV/atom and is in qualitative agreement with the direct interpolation one of 97 meV/atom. Given that the Pa3 structure is the next in the sequence of increasing pressure after the Pbcn, the ssNEB result from Fig. 5 explains the appearance of the Pbcn phase mixed with the ground-state rutile phase ($P4_2/mnm$) upon releasing pressure. Namely, the barrier of 32 meV/atom implies Pa3 will transform to Pbcn fairly quickly, while the Pbcn phase will transform to $P4_2/mnm$ at a slower rate. Interestingly, just from the coordination analysis and the calculated energy profiles one could conceive the Pa3 → Pbcn → $P4_2/mnm$ route instead of the direct Pa3 → $P4_2/mnm$.

Similarly, the ssNEB result for the Pbca → $P4_2/mnm$ transformation (see Fig. 5(d)) is clearly consistent with the conclusions that could be drawn form the coordination analysis. Namely, from the coordination of atoms this transformation would undoubtedly be considered slow, and the lowering of energy from Pbca would likely proceed along the pathways marked by the arrows in Fig. 4, that is, either through the Pa3 and then Pbcn, or directly to the Pbcn structure. As previously discussed both of these transformations can be considered rapid. This is exactly what the ssNEB predicts would happen. The Pbca would, according to ssNEB, transform rapidly into the Pbcn (barrier of 44 meV/atom) and would then continue along the Pbcn → $P4_2/mnm$ path.

As the SnO_2 results demonstrate, structure mapping and careful coordination analysis can offer qualitative guidance and accelarate the classification of the polymorphic transformation into rapid and slow. While replacing the ssNEB results with just the energy profiles calculated from the interpolation of our pathways might be tempting, one needs to remember that the barriers calculated in this way only represent the upper bounds for the true activation energy. The problem occurs if the upper bound for the activation energy is relatively large. We argue here that under these circumstances careful coordination analysis can still be useful in providing qualitative assessment as discussed for the transitions denoted by dashed lines in Fig. 4. Of course, the ssNEB in these cases would provide the ultimate answer.

We further tested our mapping algorithm and the qualitative conclusions based on coordination analysis using SiO_2 as another case study (see Supplementary Materials for details). The resulting classification based on the coordination of atoms shows fast transformations between α- and β-quartz, α- and β-cristobalite, and α- and β-tridymite. All other transformations between them and also including high-pressure moganite and stishovite would be classified as slow (coordination does not depend on the tolerance factor). This entirely geometric- and coordination of atoms- based classification reproduces qualitatively well the available knowledge of the SiO_2 polymorphs and the kinetics of polymorphic transformations between them.

IV. CONCLUSIONS

With the goal of accelerating assessment of kinetics of polymorphic transformations we present a general algorithm to map crystal structures onto each other and identify diffusionless pathways between them. The algorithm is based on the physical principles of minimizing the distance between individual atoms (diffusionless transformations) and minimizing the change in coordination of atoms (dissociation of chemical bonds) along the pathway. Application of the algorithm to well-studied unary and binary systems reliably reproduces known transformation pathways and reveals the critical role the dissociation of chemical bonds plays in identifying the fast-kinetics mapping. We show that rapid polymorphic transformations occur along pathways in which the number of bonds in the end-member structures is preserved. In ionic systems the number bonds can be approximated by the first-shell coordination whereas in strongly covalent systems, the increased bond directionality necessitates going beyond a geometric analysis to assess the bonding character along the pathway. These findings allow qualitative, quick and reliable classification of polymorphic transformations into rapid and slow just from the coordination (or bonding) analysis as we show on a number of well-studied polymorphic transformations as well as those between high-pressure phases of SnO_2 for which atomic level understanding is presently missing. For more quantitative assessments integration of our algorithm with ssNEB calculations is shown to provide a robust computational procedure for predicting kinetics of polymorphic transformations. Ultimately, the methods presented here, in combination with structure and property predictions, offer a route to identifying novel, realizable and long-lived functional materials among metastable polymorphs.

ACKNOWLEDGMENTS

This work was supported as part of the Center for the Next Generation of Materials by Design, an Energy Frontier Research Center funded by the U.S. Department of Energy, Office of Science, Basic Energy Sciences. The research was performed using computational resources sponsored by the Department of Energy's Office of Energy Efficiency and Renewable Energy and located at the

National Renewable Energy Laboratory.

* vstevano@mines.edu

[1] S. M. Woodley and R. Catlow, Nat Mater **7**, 937 (2008).
[2] A. Oganov, *Modern methods of crystal structure prediction* (Wiley-VCH John Wiley distributor, Weinheim Chichester, 2010).
[3] S. Evrenk, *Prediction and calculation of crystal structures: methods and applications* (Springer, Cham Switzerland, 2014).
[4] G. Hautier, A. Jain, S. P. Ong, B. Kang, C. Moore, R. Doe, and G. Ceder, Chemistry of Materials **23**, 3495 (2011).
[5] A. O. Lyakhov and A. R. Oganov, Phys. Rev. B **84**, 092103 (2011).
[6] S. Botti, J. A. Flores-Livas, M. Amsler, S. Goedecker, and M. A. L. Marques, Phys. Rev. B **86**, 121204 (2012).
[7] Y. Li, J. Hao, H. Liu, Y. Li, and Y. Ma, J. of Chem. Phys. **140**, 174712 (2014).
[8] H. Peng, P. F. Ndione, D. S. Ginley, A. Zakutayev, and S. Lany, Phys. Rev. X **5**, 021016 (2015).
[9] A. Jain, Y. Shin, and K. A. Persson, Nature Reviews Materials **1**, 15004 EP (2016).
[10] R. J. Needs and C. J. Pickard, APL Materials **4**, 053210 (2016).
[11] A. G. Kvashnin, A. R. Oganov, A. I. Samtsevich, and Z. Allahyari, J. Phys. Chem. Lett. **8**, 755 (2017).
[12] M. A. Zwijnenburg, F. Illas, and S. T. Bromley, Phys. Rev. Lett. **104**, 175503 (2010).
[13] M. A. Zwijnenburg and S. T. Bromley, Phys. Rev. B **83**, 024104 (2011).
[14] W. Sun, S. T. Dacek, S. P. Ong, G. Hautier, A. Jain, W. D. Richards, A. C. Gamst, K. A. Persson, and G. Ceder, Science Advances **2** (2016), 10.1126/sciadv.1600225.
[15] S. De, B. Schaefer, A. Sadeghi, M. Sicher, D. G. Kanhere, and S. Goedecker, Phys. Rev. Lett. **112**, 083401 (2014).
[16] V. Stevanović, Phys. Rev. Lett. **116**, 075503 (2016).
[17] E. Jones and V. Stevanović, arXiv preprint , arXiv:1708.09026 (2017).
[18] K. J. Caspersen and E. A. Carter, Proc. Natl. Acad. Sci. U.S.A. **102**, 6738 (2005).
[19] D. Sheppard, P. Xiao, W. Chemelewski, D. D. Johnson, and G. Henkelman, The Journal of Chemical Physics **136**, 074103 (2012).
[20] G.-R. Qian, X. Dong, X.-F. Zhou, Y. Tian, A. R. Oganov, and H.-T. Wang, Comput. Phys. Commun. **184**, 2111 (2013).
[21] M. J. Buerger, in *Phase transformations in solids*, edited by R. Smoluchowski, J. E. Mayer, and W. A. Weyl (John Wiley and Sons, New York, 1951) pp. 183–211.
[22] C. Capillas, J. M. Perez-Mato, and M. I. Aroyo, J. Phys.: Condens. Matter **19**, 275203 (2007).
[23] G. L. W. Hart and R. W. Forcade, Phys. Rev. B **77**, 224115 (2008).
[24] P. Niggli, Handbuch der Experimentalphysik **7, part 1** (1928).
[25] A. Santoro and A. D. Mighell, Acta Cryst. **A26**, 124 (1970).
[26] I. Krivy and B. Gruber, Acta Cryst. **A32**, 297 (1976).
[27] H. W. Kuhn, Naval Research Logistics Quarterly **2**, 83 (1955).
[28] A. Sadeghi, S. A. Ghasemi, B. Schaefer, S. Mohr, M. A. Lill, and S. Goedecker, J. Chem. Phys. **139**, 184118 (2013).
[29] D. C. Lonie and E. Zurek, Comput. Phys. Comm. **183**, 690 (2012).
[30] L. Yang, S. Dacek, and G. Ceder, Phys. Rev. B **90**, 054102 (2014).
[31] L. Zhu, M. Amsler, T. Fuhrer, B. Schaefer, S. Faraji, S. Rostami, S. A. Ghasemi, A. Sadeghi, M. Grauzinyte, C. Wolverton, and S. Goedecker, J. Chem. Phys. **144**, 034203 (2016).
[32] `https://github.com/pylada/pylada-polymorph-pathfinder`.
[33] V. Stevanović, S. Lany, X. Zhang, and A. Zunger, Phys. Rev. B **85**, 115104 (2012).
[34] J. P. Perdew, K. Burke, and M. Ernzerhof, Phys. Rev. Lett. **77**, 3865 (1996).
[35] P. E. Blöchl, Phys. Rev. B **50**, 17953 (1994).
[36] G. Kresse and J. Furthmüller, Comput. Mater. Sci. **6**, 15 (1996).
[37] J. Klime, D. R. Bowler, and A. Michaelides, Journal of Physics: Condensed Matter **22**, 022201 (2010).
[38] G. Henkelman, B. P. Uberuaga, and H. Jónsson, The Journal of Chemical Physics **113**, 9901 (2000).
[39] M. Catti, Phys. Rev. Lett. **87**, 035504 (2001).
[40] M. S. Miao and W. R. L. Lambrecht, Phys. Rev. B **68**, 092103 (2003).
[41] F. Decremps, J. Pellicer-Porres, F. Datchi, J. P. Itié, A. Polian, F. Baudelet, and J. Z. Jiang, Applied Physics Letters **81**, 4820 (2002).
[42] S. Limpijumnong and W. R. L. Lambrecht, Phys. Rev. Lett. **86**, 91 (2001).
[43] D. R. Trinkle, R. G. Hennig, S. G. Srinivasan, D. M. Hatch, M. D. Jones, H. T. Stokes, R. C. Albers, and J. W. Wilkins, Phys. Rev. Lett. **91**, 025701 (2003).
[44] R. Z. Khaliullin, H. Eshet, T. D. Kühne, J. Behler, and M. Parrinello, Nat. Mater. **10**, 693 (2011).
[45] P. Xiao and G. Henkelman, The Journal of Chemical Physics **137**, 101101 (2012).
[46] V. Stevanović, M. d'Avezac, and A. Zunger, Phys. Rev. Lett. **105**, 075501 (2010).
[47] V. Stevanović, M. d'Avezac, and A. Zunger, Journal of the American Chemical Society **133**, 11649 (2011).
[48] S. R. Shieh, A. Kubo, T. S. Duffy, V. B. Prakapenka, and G. Shen, Phys. Rev. B **73**, 014105 (2006).
[49] S. Das and V. Jayaraman, Prog. Mater Sci. **66**, 112 (2014).
[50] L.-G. Liu, Science **199**, 422 (1978).
[51] Complete information about all SnO_2 polymorphs, their relative energies as well as the energy profiles for the transformations between them are provided in Supplementary Information.